# Prediction of the Degree of Bonding in the Extrusion Deposition Additive Manufacturing Process of Semi-Crystalline Polymer Composites

Eduardo Barocio, Bastian Brenken, Anthony Favaloro, Miguel Ramirez, Jorge Ramirez, and R. Byron Pipes

Composites Manufacturing and Simulation Center

Purdue University

**Abstract**: *The Extrusion Deposition Additive Manufacturing (EDAM) process is a manufacturing process used to produce three-dimensional objects made by deposition of molten polymer composite in a layer-by-layer fashion. Printing with fiber reinforced, semi-crystalline polymers provides for the manufacture of molds that can be used in high-temperature composite prototype molding applications. Further, the EDAM is scalable and can provide printed geometries in the centimeter to meter scales. However, in plane (X-Y) fiber orientation of the extrudate results in mechanical properties in the stacking orientation (Z) that are governed by the bond formed between adjacent extrudate layers. The quality of this interlayer bond is strongly influenced by the processing conditions, namely temperature and printing history. Therefore, simulation tools are required to predict the influence of printing conditions on the interlayer bond strength and to optimize printing parameters for maximum interlayer bond strength. The degree of bonding is defined in the context of this work as the ratio of recovered mode-I critical energy release rate to the critical energy release rate of a fully bonded interface. The degree of bonding is predicted by coupling an autohesion model with the temperature history and the evolution of crystallinity. This method has been implemented in a UMATHT user subroutine and is used together with functionalities deployed in Abaqus 2017 for simulating additive manufacturing methods to predict the evolution of the degree of bonding in the EDAM process. Finally, the predictions for degree of bonding for multiple processing conditions are validated with experimental measurements.*

## 1. Introduction

The rapid evolution of technologies and materials for large-scale polymer additive manufacturing (AM) or 3D-Printing has significantly increased the number of applications leveraging the design flexibility gained with this technology. Extrusion Deposition Additive Manufacturing (EDAM) is a screw extrusion-based method for fabricating of three-dimensional geometries in a layer-by-layer fashion. Unlike methods that use filament feedstock material such as the Fused Deposition Modeling (FDM) and Fused Filament Fabrication (FFF), EDAM utilizes pelletized feedstock

material, thereby enabling printing with highly filled, short-fiber-reinforced polymers. By reinforcing printing materials with discontinuous carbon fiber, the stiffness of the polymer is increased and the coefficient of thermal expansion is reduced, especially along the direction of the fibers. Such an advancement in printing materials made feasible to up-scaling the size of the objects that can be manufactured with this technology (Love, et al., 2014). The Composites Additive Manufacturing Research Instrument (CAMRI) was developed at Purdue University to investigate the EDAM process and to validate simulations of the printing process. Compaction mechanisms such as tampers or rollers have been adopted in the EDAM process to consolidate the beads of molten material as it leaves the printing nozzle. CAMRI is equipped with a tamper system that utilizes a vibrating plate that surrounds the printing nozzle to compact the beads of molten material during deposition. The squeeze flow caused by tamping the molten material reorients fibers in the extruded bead to an in-plane dominated fiber orientation distribution, thereby giving rise to anisotropy in the mechanical, transport and flow properties.

The continuous deposition of molten material onto either a previously deposited material layer or a build plate leads to temperature gradients in the printed part. As a result, thermal strains are introduced incrementally layer-by-layer, thereby giving rise to residual stresses and deformation during and after printing.

A recurring issue in the EDAM process of a composite part has been delamination of printed layers. This arises primarily due to the combination of low interlayer bond strength and residual stresses. In order to allow for the optimization of print strategies for minimization or elimination of interlayer cracking, the implementation of a method for predicting the interlayer bond strength based on polymer diffusion, temperature and crystallinity is presented in this paper. This work represents the first step toward predicting delamination during printing and during service of printed components. The degree of bonding is a measure of the interlayer bond strength and is defined as the ratio of the recovered mode-I critical energy release rate (CERR) to the mode-I CERR measured from a joint bonded under ideal conditions. In addition to describing the implementation of this method, predictions of the degree of bonding are validated against values measured experimentally through test of double cantilever beam (DCB) specimens printed with 50% by weight carbon fiber reinforced polyphenylene sulfide (PPS).

## 1.1    Process Simulations of the EDAM in Abaqus

The physical process of continuously depositing beads of molten material on either a printed substrate or on a build plate is simulated in Abaqus/Standard by sequentially activating elements in a part-unspecific mesh (Abaqus Users Manual, 2017). The sequence of events used for activating the elements is provided through the event series which is a temporal description of the printing trajectory. An algorithm that searches for elements contained within a sphere moving along a given printing trajectory is used to determine the activation time and the local material orientation for each element (Favaloro, 2017). The pre-computed activation time is then used in the new user subroutine UEPActivationVol to activate elements at each time increment of the printing simulation (Abaqus Users Manual, 2017). Since the exposed surfaces in a model change as new elements are activated in the printing simulations, the exposed surfaces must be updated at each time increment to capture correctly the convective and radiative heat losses. The process of

2

redefining the surface boundary conditions is managed automatically with the new options FFS and RFS in the $*FILM$ and $*Radiate$ keywords, respectively (Abaqus Users Manual, 2017).

The flow of printing material through converging zones of the printing nozzle align the fibers in the print direction (Heller, 2016). As stated above, the tamping process leads to an in-plane dominated fiber orientation distribution within the printed bead, whose effects in the material properties are captured by defining orthotropic material properties. Using the printing trajectory informed through the event series, Favaloro et al. developed an algorithm to assign material orientations in the user subroutine ORIENT (Favaloro, 2017).

These new capabilities in Abaqus have enabled not only simulation of the EDAM process, but also the anisotropic properties critical to accurate prediction of the evolution of temperature, deformation and residual stress.

## 2. Fusion Bonding of Semi-Crystalline Polymer Composites

Fundamentals of fusion bonding of polymeric interfaces are described in this section to introduce the method implemented for predicting the degree of bonding and the assumptions made with this approach. The process of bonding two polymeric surfaces involves the diffusion of polymer chains through the interface formed by both surfaces. For the case of the EDAM process, these two surfaces correspond to adjacent layers. The diffusion process of polymer chains is strongly influenced by temperature and the development of crystallinity. While thermal energy facilitates the diffusion of polymer chains by increasing Brownian motion, the steep increase in viscosity with crystallization hinders the diffusion of polymer chains in semi-crystalline polymers. The process of fusion bonding polymers has been described in terms of five sequential stages, namely surface rearrangement, surface approach, wetting, diffusion, and randomization (Wool, 1981). However, the steps of surface rearrangement, surface approach and wetting occur instantaneously in the EDAM process due to the process of compacting the extruded beads with the tamper. As a result, intimate contact between the bonding surfaces is achieved instantaneously. Upon establishment of intimate contact, polymer chains begin to diffuse through the interface until these are fully randomized across the interface. At this point, the initially visible interface vanishes and the mechanical properties approach those of the bulk polymer. This condition corresponds to a degree of autohesion equal to unity. As a consequence of the prerequisite of attaining intimate contact between the bonding surfaces for polymer diffusion, the degree of bonding is defined as the convolution of the degree of intimate contact and the degree of autohesion.

Since the degree of bonding is proportional to the number of chains diffused across the interface, this descriptor can be used to quantify the interlayer strength developed during the EDAM process. The process of autohesion has been described by scaling arguments of the theory of polymer dynamics developed by De Gennes (De Gennes, 1971). Utilizing the concepts of polymer reptation developed by De Gennes, Prager and Tirrel derived expressions to describe the evolution of the density of polymer chains across a polymeric interface. This demonstrated the relationship between polymer dynamics and the evolution of interfacial properties (Prager, 1981). Healing experiments carried out by several authors also confirmed the same time dependence on the recovered strength predicted by scaling arguments of polymer dynamics (Tirrell, 1984; Jud, 1981). For the case of semi-crystalline polymers, experimental results from Smith et al. (Smith, 2001)

and Zanetto et al. (Zanetto, 2001) have demonstrated the importance of developing crystallinity through a fusion bonded interface. Hence, based on these previous experimental observations and the effects of polymer crystallization on the diffusion of polymer chains, an approach that couples an autohesion model with the evolution of crystallinity and temperature has been developed to predict the degree of bonding in semi-crystalline polymers (Barocio, 2017). Figure 1 illustrates the deposition process of an extruded bead and the phenomena involved in the fusion bonding
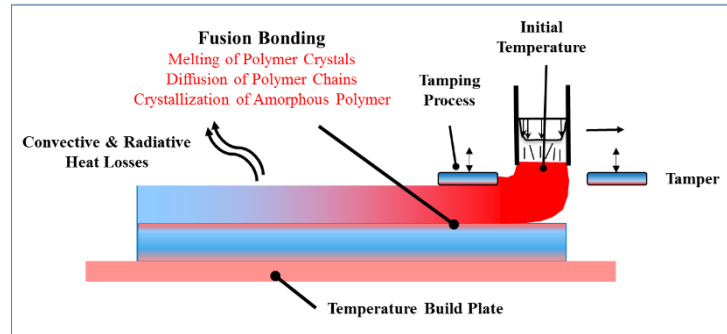


**Figure 1. Overview of the phenomena participating in the fusion bonding of semi-crystalline polymer composites during the EDAM process.**

process.

The evolution of crystallinity is described through two models coupled with a temperature condition to satisfy the thermodynamics of polymer melting. The first model describes the development of crystallinity whereas the second model describes the melting of polymer crystals. The evolution of crystallinity is then used to limit the development of the degree of bonding which is described through a non-isothermal autohesion model. This approach for predicting the degree of bonding is based on coupling models of polymer diffusion and crystallization and have been implemented in a UMATHT user subroutine.

## 2.1    Polymer Diffusion

The process of diffusing polymer chains through the interface formed by two adjacent layers in the EDAM process is carried out under highly non-isothermal conditions. Thus, the non-isothermal autohesion model derived by Yang and Pitchumani (Equation 1) was used to model the evolution of the degree of bonding $D_b$ (Yang, 2003). As stated above, $D_b$ represents a recovered fraction of the mode-I CERR ($G_1/G_{1_\infty}$). Since the degree of intimate contact is achieved instantaneously by tamping the extruded beads, the degree of bonding is described directly by the degree of autohesion as shown in Equation 1. The reptation time is replaced by a welding time $t_{wel}$ in Equation 1 since only a portion of the chain length needs to diffuse through the interface to fully recover the interlayer properties (Wool, 1981). This autohesion model has been utilized successfully in other non-isothermal manufacturing processes such as automatic tape placement of composite prepreg to describe the degree of autohesion (Grouve, 2013).

4

$$D_b(T, t) = \frac{G_1(T,t)}{G_{1\infty}} = \left[\int_0^t \frac{1}{t_{wel}(T(\tau))} d\tau\right]^{\frac{1}{2}} \tag{1}$$

The welding time $t_{wel}$ has a dependence on temperature that can be captured with the Arrhenius expression in Equation 2. The activation energy $E_A$ and the pre-exponential factor $A$ in the Arrhenius expression are characterized with non-isothermal bonding experiments.

$$t_{wel}(T(\tau)) = A exp\left(\frac{E_A}{RT(\tau)}\right) \tag{2}$$

## 2.2    Crystallization and Melting

As the polymer is cooled from the molten state, a physical transition occurs in the polymer giving rise to exothermal heat generation and volumetric contraction. Polymer crystallization is a two-step process involving nucleation and growth. Crystal nucleation is driven by the difference in temperature from the melt, whereas the growth is diffusion controlled. Further, the surface of the carbon fiber can function as nucleation sites for polymer crystals, thereby reducing the amount of cooling required for nucleation which in turn accelerates the crystallization kinetics. As a result, the crystallization kinetics are defined as the combination of the rapid nucleation of polymer crystals on the surface of the fibers and the diffusion-controlled grow of polymer crystals. Cooling rate also affects crystallization kinetics by introducing an induction time that increases with cooling rate.

Since the EDAM process with carbon fiber-reinforced, semi-crystalline polymers is highly non-isothermal and fibers affect heat transfer and crystallization kinetics, a dual crystallization mechanism and non-isothermal kinetics model is required for capturing this combined behavior. Hence, the crystallization kinetics model developed by Velisaris and Seferis was utilized (Velisaris, 1986). Each of the mechanisms controlling the crystallization kinetics are captured through the integral expressions $F_{vc_i}, i = 1,2$, and the contribution of each mechanism to the crystallization rate is controlled by the weight factors $w_i, i = 1,2$ as described by Equation 3. The weight factors satisfy the condition that their sum is always equal to unity. The product of the weighted sum of the two crystallization mechanisms and the maximum degree of crystallinity $X_{vc_\infty}$ yield the degree of crystallinity.

$$X_{vc}(T, t) = X_{vc\infty}\left(w_1 F_{vc_1} + w_2 F_{vc_2}\right) \tag{3}$$

Each mechanism $F_{vc_i}$ contributing to the crystallization rate is described by the integral expression in Equation 4 where the parameters $C_{1_i}$ capture the temperature dependence on the crystallization rate, and $C_{2_i}$ describe the temperature dependence on the crystal growth for each mechanism. Similarly, $C_{3_i}$ is related to the enthalpy of nucleation in each mechanism.

$$F_{vc_i} = 1 - exp\left\{-C_{1_i}\int_0^t T \cdot exp\left[\frac{-C_{2_i}}{(T-T_g+T_{c_i})} - \frac{C_{3_i}}{\left(T\left(T_{m_i}-T\right)^2\right)}\right] n_i \tau^{n_i-1} d\tau\right\} \tag{4}$$

$$i = 1, 2$$

The four temperatures $T, T_g, T_{c_i}$ and $T_{m_i}$ used in this model represent the temperature of the process, the glass transition temperature, the melting temperature, and an empirically determined

5

temperature limiting the diffusion term in Equation 4, respectively. The $n_i$ represent the two Avrami coefficients characterized with isothermal crystallization experiments and $t$ is time.

The process of depositing beads of molten material onto previously deposited material can lead to local re-melting of polymer crystals in the previously deposited material. Furthermore, re-melting of polymer crystals in the vicinity of the interface is required to enable diffusion of polymer chains through the interface and subsequently to develop crystallinity through the interface. Experimental characterization of the melting behavior of polymer crystallized from the melt at cooling rates relevant for the EDAM process indicated that the melting behavior is virtually independent of the heating rate. Thus, the non-isothermal model in Equation 5 developed by Greco and Maffezzoli was utilized to describe the melting process of polymer crystals (Greco, 2003). This model assumes a statistical distribution of crystal lamellar thickness with a sharpness factor $k_{mb}$ and a distribution factor $d$. The temperature $T_C$ corresponds to the peak in the heat flow signal characterized through differential scanning calorimetry.

$$\frac{dX_{vc}}{dT} = k_{mb}\{exp[-k_{mb}(T - T_c)]\} \cdot (1 + (d - 1) \, exp[-k_{mb}(T - T_c)])^{\frac{d}{1-d}} \quad (5)$$

In order to satisfy the thermodynamics relating the lamellar thickness to the melting temperature of the polymer crystals, the transition between the melting and the crystallization kinetics models is controlled by the onset temperature of melting $T_m^*$. The melting model controls the evolution of crystallinity when the temperature is above $T_m^*$, whereas the crystallization model dominates the evolution of crystallinity in the opposite case. These conditions are summarized in Equation 6.

$$X_{vc}(T, t) = \begin{cases} T > T_m^*, & X_{vc}(T) - Melting \\ T \leq T_m^*, & X_{vc}(T, t) - Crystallization \end{cases} \quad (6)$$

$$X_{vc} \in [0 \; 1]$$

## 3.  Implementation in Abaqus

The degree of bonding is predicted in the EDAM process simulations by implementing the models describing polymer crystallization, polymer melting and polymer autohesion in a UMATHT user subroutine. This subroutine is called at each material point and at every global iteration. The information passed in to the subroutine is used to compute the increment of the degree of bonding, crystallinity and latent heat of crystallization. The simulation flowchart in Figure 2 summarizes the method implemented in a UMATHT that captures the couplings between the multiple phenomenological models described above in order compute the degree of bonding in the EDAM process simulations.

**Figure 2. Flowchart of the method implemented in the UMATHT subroutine to predict the degree of bonding.**

The crystallization and melting models were previously implemented by Brenken et al. (Brenken, 2017). Nevertheless, this work extends the previous implementation by redefining the transition between the melting and crystallization models and by strongly coupling the evolution of crystallinity with the heat transfer analysis. In the present work, the heat released during polymer crystallization and the heat absorbed during melting of polymer crystals is considered in the heat transfer analysis. With regards to the evolution of crystallinity, the melting model controls the evolution of crystallinity if the temperature is above $T_m^*$, whereas the crystallization model controls the evolution of crystallinity if the temperature is below $T_m^*$ as depicted in the flowchart of Figure 2. The degree of crystallinity is bounded such that $0 \leq X_{vc} \leq 0.84$.

To implement the autohesion model, the integral in Equation 1 is approximated numerically using Simpson's 3/8 rule with a step size $h$ as shown in Equation 7. The limits of the integral in the left-hand side (LHS) are defined from the time the element is activated in the process simulation $t_{act}$, to the current time $t$. The numerical integration on the right-hand side (RHS) is carried out at each time increment $\Delta t$.

$$\int_{t_{act}}^{t} \frac{1}{t_{weld}(T(\tau))} d\tau \approx \sum_{i=1}^{t/\Delta t} \frac{3h}{8} \left( f(\tau_0) + 3f(\tau_1) + 3f(\tau_2) + f(\tau_3) \right) \tag{7}$$

The functions $f(\tau_n)$ are replaced by the inverse of the welding time evaluated at time increments of $h$ (Equation 8). The temperature $T_n$ used for each of the time increments $h$ is linearly interpolated from the temperature passed into the UMATHT at the beginning and at the end of a time increment $\Delta t$. It should be noticed that $h \ll \Delta t$.

$$f(\tau_n) = \frac{1}{t_{weld}(T_n(\tau_n))} \quad n = 0, 1 \dots 3 \tag{8}$$

For the case of long time increments $\Delta t$, the approximation of the time integral in Equation 7 is improved by carrying out sub-increments such that $\Delta t_{sub} \ll \Delta t$. The final expression for the degree of bonding given by Equation 9 is obtained by substituting Equation 7 into Equation 1.

$$D_b(T,t) = \left[\sum_{i=1}^{t/\Delta t} \frac{3h}{8} \left(f(\tau_0) + 3f(\tau_1) + 3f(\tau_2) + f(\tau_3)\right)\right]^{\frac{1}{2}} \qquad (9)$$

## 4.   Results and Validation

Validating the predictions of the degree of bonding made with the approach implemented in this paper required the experimental measurement of the critical energy release rate (CERR) at different degrees of bonding. Since the degree of bonding is defined as a ratio of mode-I CERR, double cantilever beam (DCB) specimens with different degrees of bonding were printed in the CAMRI system with 50% by weight of carbon fiber PPS. Six different process conditions were used to prepare specimens that resulted into six different degrees of bonding. Furthermore, the dimensions of the specimens were designed to minimize temperature gradients that could lead to variations of degree of bonding along the plane of crack propagation. The process conditions varied across the specimens were the temperature of the build plate and the dwell time between the layers defining the plane of crack propagation. DCBs were tested under fix-grip conditions to measure the CERR.

To validate the predictions of the degree of bonding, the process conditions used for manufacturing the DCBs were simulated in Abaqus/Standard with the functionalities for additive manufacturing described above. Figure 3-A shows the temperature distribution predicted in the simulation of the printing process for one of the DCBs. Additionally, the temperature evolution up to crystallization onset was extracted from nodes located in the plane of crack propagation and plotted for the six printing conditions in Figure 3-B. Although the degree of bonding is computed
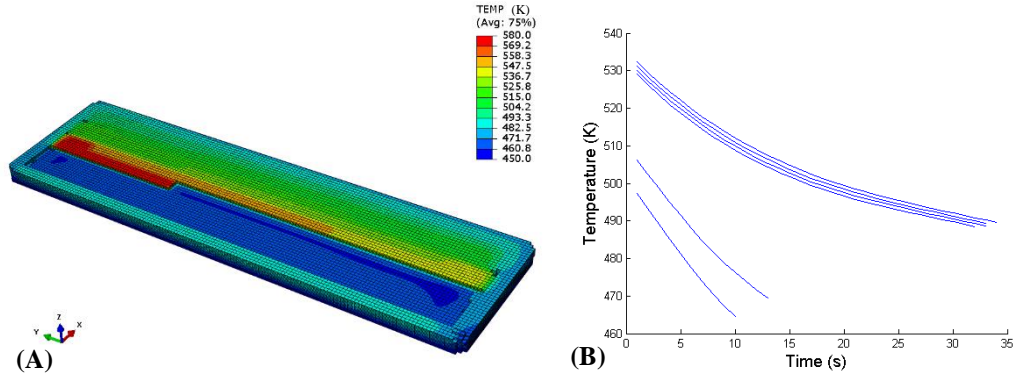


**Figure 3. A) Temperature distribution during printing process of double cantilever beam specimen. B) Temperature history until the onset of crystallization extracted from nodes located at the plane of crack propagation for each of the six printing conditions used for validation.**

8
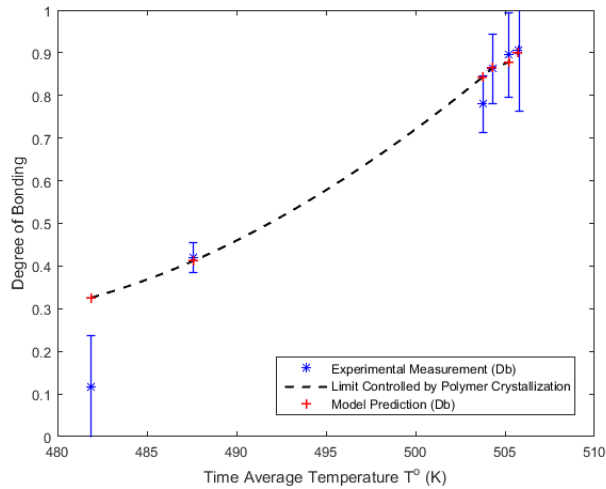
**Figure 4. Comparison of the experimentally measured and the predicted degrees of bonding.**

for the entire model, this is only relevant at the nodal points located along the interface between two layers. Future refinements of this approach include implementing the autohesion model in a UINTER user subroutine.

Since different degrees of bonding resulted from each of the temperature histories plotted in Figure 3-B, the time averaged temperature was computed for each of the temperature histories. This way, the degree of bonding resulting from non-isothermal bonding conditions can be compared systematically. The plot in Figure 4 compares the experimental measurements of the degree of bonding and the degree of bonding predicted in the process simulations. The good correlation between the predicted and experimentally measured degree of bonding validates the approach described above for predicting the degree of bonding in the EDAM process. Further, since the factor limiting the evolution of degree of bonding is the crystallization onset, the dashed line in Figure 4 outlines the maximum degree of bonding achieved in a range of time average temperature of 480 to 505 K.

## 5. Conclusions

A method to predict the degree of bonding between layers in the EDAM process with semi-crystalline polymer composites was implemented in a UMATHT user subroutine. Due to the retardation of the diffusion of polymer chains caused by the polymer crystallization, the evolution of crystallinity was found to be the factor limiting the evolution of the degree of bonding. The degree of bonding is characterized as the ratio of the recovered mode-I CERR to the maximum CERR measured from a fully healed interface. Experimental measurements of mode-I CERR using DCB specimens validates the method described in this paper to predict the evolution of the degree of bonding.

9

Modeling the evolution of the degree of bonding between layers during the EDAM process is the first step toward predicting cracking and delamination during manufacturing or during service of printed components. Further characterization is required to capture the temperature dependence on the CERR and future work includes informing a cohesive zone model with the process controlled degree of bonding to predict delamination. Finally, process simulations are essential predictive tools required to advance the additive manufacturing technologies by reducing the empirical determination of processing windows.

## 6.  References

Abaqus Users Manual. (2017). Abaqus Online Documentation Server, Abaqus 2017. (Dassault Systemes) Retrieved February 15, 2018, from http://50.16.225.63/

Barocio, E., Brenken, B., Favaloro, A., Ramirez, J., Kunc, V., & Pipes, R. B. (2017). "Fusion Bonding Simulations of Semi-Crystalline Polymer Composites in the Extrusion Deposition Additive Manufacturing Process". Proceedings of the American Society for Composites—Thirty-second Technical Conference.

Brenken, B., Barocio, E., Favaloro, A. J., & Pipes, R. B. (2017). "Simulation of Semi-Crystalline Composites in the Extrusion Deposition Additive Manufacturing Process". Science in the Age of Experience.

De Gennes, P.-G. (1971). "Reptation of a Polymer Chain in the Presence of Fixed Obstacles". The Journal of Chemical Physics, 55(2), 572-579.

Favaloro, A. J., Brenken, B., Barocio, E., & Pipes, R. B. (2017). "Simulation of Polymeric Composites Additive Manufacturing using Abaqus". Science in the Age of Experience.

Greco, A., & Maffezzoli, A. (2003). "Statistical and Kinetic Approaches for Linear low-density Polyethylene Melting Modeling". Journal of Applied Polymer Science, 89(2), 289-295.

Grouve, W., Warnet, L., Rietman, B., Visser, H., & Akkerman, R. (2013). "Optimization of the Tape Placement Process Parameters for Carbon–PPS Composites". Composites Part A: Applied Science and Manufacturing , 50, 44-53.

Heller, B. P., Smith, D. E., & Jack, D. A. (2016). "Effects of Extrudate Swell and Nozzle Geometry on Fiber Orientation in Fused Filament Fabrication Nozzle Flow" . Additive Manufacturing , 12, Part B, 252-264.

Jud, K., Kausch, H. H., & Williams, J. G. (1981). "Fracture Mechanics Studies of Crack Healing and Welding of Polymers". Journal of Materials Science, 16(1), 204-210.

Love, L. J., Kunc, V., Rios, O., Duty, C. E., Elliott, A. M., Post, B. K., . . . Blue, C. A. (2014). "The importance of Carbon Fiber to Polymer Additive Manufacturing". Journal of Materials Research, 29, 1893-1898.

Prager, S., & Tirrell, M. (1981). "The Healing Process at Polymer–Polymer Interfaces". The Journal of Chemical Physics, 75(10), 5194-5198.

Smith, G. D., Plummer, C. J., Bourban, P.-E., & Månson, J.-A. E. (2001). "Non-isothermal Fusion Bonding of Polypropylene" . Polymer , 42(14), 6247-6257.

Tirrell, M. (1984). "Polymer Self-Diffusion in Entangled Systems". Rubber Chemistry and Technology, 57(3), 523-556.

Velisaris, C. N., & Seferis, J. C. (1986). "Crystallization Kinetics of Polyetheretherketone (peek) Matrices". Polymer Engineering & Science, 26(22), 1574-1581.

Wool, R. P., & O'Connor, K. M. (1981). "A Theory Crack Healing in Polymers". Journal of Applied Physics, 52(10), 5953-5963.

Yang, F., & Pitchumani, R. (2003). "Nonisothermal Healing and Interlaminar Bond Strength Evolution During Thermoplastic Matrix Composites Processing". Polymer Composites, 24(2), 263-278.

Zanetto, J.-E., Plummer, C. J., Bourban, P.-E., & Månson, J.-A. E. (2001). "Fusion Bonding of Polyamide 12". Polymer Engineering & Science, 41(5), 890-897.